nature biomedical engineering

ARTICLES

PUBLISHED: 10 MAY 2017 | VOLUME: 1 | ARTICLE NUMBER: 0070

Closed-loop control of circulating drug levels in live animals

P. L. Mage[1†], B. S. Ferguson[2†], D. Maliniak[2], K. L Ploense[2,3], T. E. Kippin[2,3,4,5] and H. T. Soh[1,2,6,7*]

Current methods of drug dosing rely on physical parameters (such as sex, age and weight) that do not account for genetic and physiological differences among individual patients. These differences can greatly affect how drugs are processed in the body and can result in ineffective underdosing or toxic overdosing. Here, we describe a generalizable closed-loop system consisting of a biosensor, controller and infusion pump, and a model of drug pharmacokinetics that continuously monitors and adjusts the concentration of a given drug in the body. As proof of concept, we demonstrate that the system can maintain the concentration of doxorubicin—a widely used chemotherapy drug—in live rabbits and rats at any desired set point and in real time, while automatically compensating for large pharmacokinetic differences among individual animals and stabilizing dramatic perturbations arising from acute drug–drug interactions. The feedback-loop system opens up the possibility of tightly controlled, patient-specific dosing of chemotherapeutics and other drugs within narrow therapeutic windows.

Current protocols for predicting the optimal drug dose for a patient generally rely on easily obtained physical parameters, such as sex, age, body weight or body surface area[1–3]. Unfortunately, these parameters do not account for individual differences in pharmacokinetics (PK; how the drug is processed by the body) and pharmacodynamics (how the body is affected by the drug), which can lead to ineffective underdosing or toxic overdosing[4,5]. This is an especially important problem for drugs that exhibit narrow therapeutic windows within which the concentration of drug in the bloodstream is both effective and safe, such as chemotherapeutics[6,7], immunosuppressants[8,9], anticoagulants[10], insulin[11] and anaesthetics[12].

To date, two broad strategies have been developed to personalize drug dosing. In the first, an optimal dose for a given patient is calculated in advance based on their germ-line genomic profile (that is, pharmacogenetic testing[13]) or direct measurement of the patient's PK (that is, therapeutic drug monitoring[14]). Unfortunately, these methods are limited to only a small set of drugs[15,16]. Furthermore, they are costly[17,18], and are often too time-consuming to enable timely treatment in the clinic[19]. The second strategy aims to dynamically compensate for individual differences in PK and pharmacodynamics by adjusting drug delivery based on physiological feedback signals, such as blood pressure, electroencephalography or blood glucose concentration (reviewed in ref. [20]). Unfortunately, this strategy is not broadly applicable, because most drugs do not produce an immediate physiological signal that can be used for feedback control. The strategy is currently applicable only to cardiovascular drugs[21], anaesthetics[22] and insulin[23]. There is currently no reliable approach for the precise, individualized dosing of the many other drugs with narrow therapeutic windows.

Here we demonstrate a generalizable technology that achieves individualized delivery of therapeutic agents by directly monitoring and controlling the circulating concentration of drugs *in vivo* in real time. To the best of our knowledge, this is the first demonstration of direct, continuous control of drug concentrations in the body. To achieve this, our system performs real-time processing of signals generated from a greatly improved version of an aptamer-based biosensor, previously described by our group[24], and then uses the resulting data to achieve closed-loop feedback control of *in vivo* drug concentration. As proof of concept, we used our closed-loop infusion control system to control the concentration of doxorubicin (Dox) in live rabbits and rats. We chose Dox because it is a widely used chemotherapy drug that is difficult to dose because it has a narrow therapeutic window[25], and its PK and pharmacodynamics can vary widely among patients[2,26–29]. Using our system, we demonstrate the unprecedented capability to automatically compensate for differences in PK between individual animals where traditional dosing approaches have failed. Furthermore, we demonstrate the capability to maintain the desired drug concentration even in the presence of severe PK disturbances, such as acute drug–drug interactions. Given the modular nature of our system, we believe it could be configured to achieve a similar degree of precision dose control for a broad range of other small molecule drugs.

Results

Design of the closed-loop system. Our closed-loop infusion control system combines three elements to achieve closed-loop feedback control (Fig. 1a): (1) a biosensor, which measures the concentration of drug in the bloodstream; (2) a controller, which uses a proportional–integral–derivative (PID)[30] feedback algorithm to determine the rate of drug delivery needed to achieve the desired concentration; and (3) an infusion pump, which delivers the drug at the rate specified by the controller. This general configuration can be used to control virtually any small -molecule intravenous drug for which an aptamer probe is available, but we optimized our system's performance to match the specific clinical requirements of Dox in terms of response time, stability and robustness[30]. First, our system was designed to have a rapid response time, capable of reaching and maintaining changes in the concentration set point

[1]Department of Materials, University of California, Santa Barbara, California 93106, USA. [2]Institute for Collaborative Biotechnologies, University of California, Santa Barbara, California 93106, USA. [3]Department of Psychological and Brain Sciences, University of California, Santa Barbara, California 93106, USA. [4]Neuroscience Research Institute, University of California, Santa Barbara, California 93106, USA. [5]Department of Molecular, Cellular and Developmental Biology, University of California, Santa Barbara, California 93106, USA. [6]Department of Electrical Engineering, Stanford University, Stanford, California 94305, USA. [7]Department of Radiology, Stanford University, Stanford, California 94305, USA. [†]Present addresses: Department of Electrical Engineering, Stanford University, Stanford, California 94305, USA (P.L.M.); Aptitude Medical Systems, Inc., Santa Barbara, California 93105, USA (B.S.F.). *e-mail: tsoh@stanford.edu

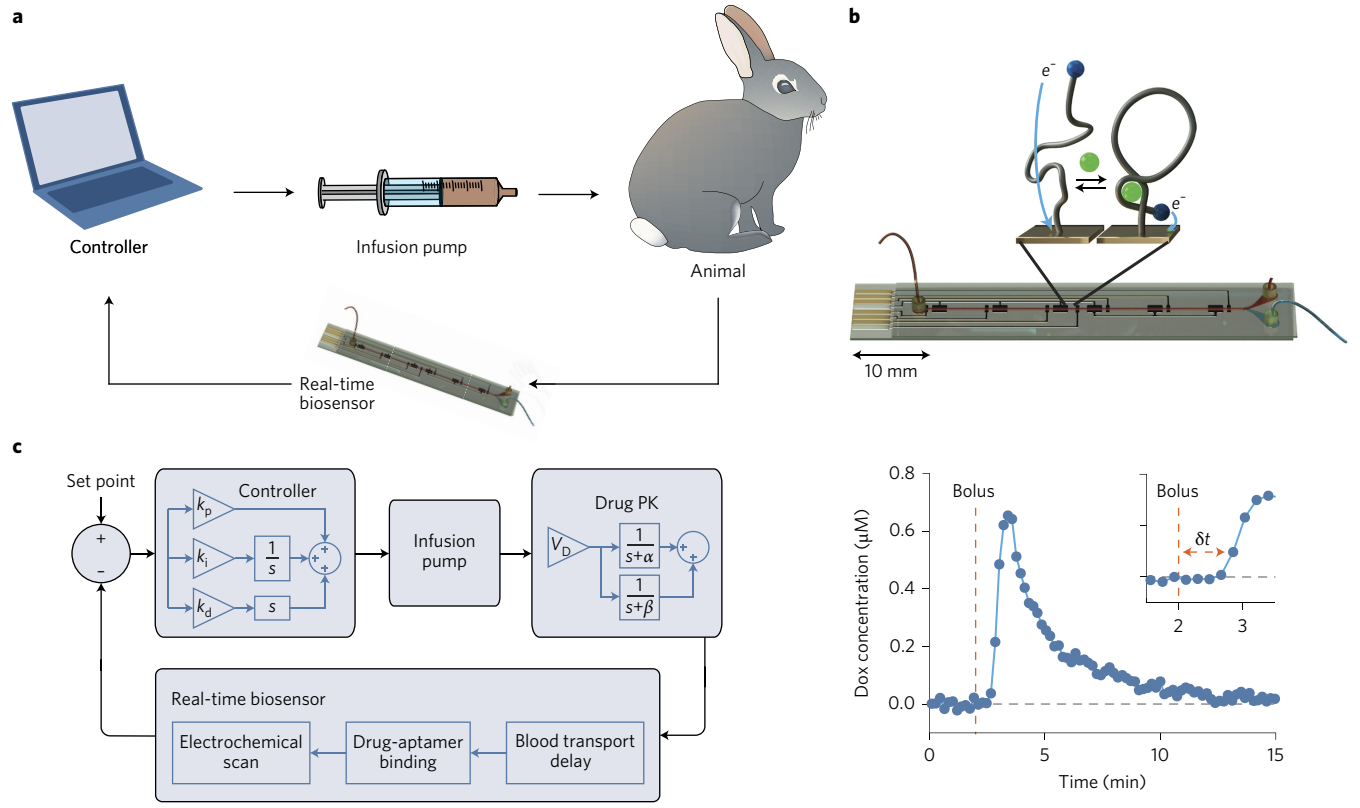

Figure 1 | Closed-loop control of *in vivo* drug levels with real-time biosensing. a, As a programmable infusion pump injects drug into the animal, the bloodstream is sampled continuously by our real-time biosensor. The resulting electrochemical measurements of drug concentration are analysed by our feedback controller, which calculates the infusion rate needed to maintain the desired circulating drug set point at any given time and automatically adjusts the infusion rate accordingly. **b**, Top: the real-time biosensor incorporates shape-shifting electrochemical aptamer probes into a microfluidic device that allows continuous measurement of drug directly from whole blood. These probes change conformation upon binding to the target molecule (green), causing a change in the rate of electron (e^-) transfer from an electrochemical redox marker (blue) to a microfabricated electrode. Bottom: our real-time biosensor enables continuous observation of Dox PK in live rabbits with a point-to-point time resolution of 11 s and a measurement lag (δt) of 0.8 min, as shown in the inset. The vertical dashed lines indicate the time of Dox bolus injection. Measurements from a single rabbit (blue dots) are shown; grey dashed lines highlight 0 μM Dox. **c**, The feedback loop can be modelled *in silico*. This model comprises: the controller with proportional, integral and derivative gains k_p, k_i and k_d; the infusion pump; drug PK, with an effective dilution volume V_D, and exponential α- and β-phase elimination rates; and the real-time biosensor. *s* denotes the complex Laplace variable in transfer-function form. Simulations based on this model enable *in silico* controller simulation and tuning for control *in vivo*.

within 10 min, the average α-phase clearance time of Dox in circulation[31–34]. Second, the system was configured to maintain stable Dox concentrations for more than 2 h of continuous operation, reflecting the typical infusion periods used during Dox chemotherapy[31]. Third, we designed our system to achieve robust control over a wide range of PK, because plasma clearance rates of Dox can vary more than tenfold from patient to patient[27]. Achieving this response time, stability and robustness required careful design and optimization of both the biosensor and the controller.

To meet these requirements, we needed to make considerable improvements to the design of our previously reported biosensor (Fig. 1b)[24]. Briefly, this biosensor uses electrochemically tagged aptamer probes (reviewed in ref. [35]) that are designed to undergo a reversible conformation change on binding to their drug target, causing a change in redox current between the electrochemical tag and an electrode. This electrochemical measurement occurs within a microfluidic device (fabrication details in Supplementary Fig. 1) that continuously samples a small volume of blood directly from the animal's bloodstream, achieving rapid, quantitative and specific measurement of *in vivo* drug concentration. In the initial applications of this sensor, the data could be processed *a posteriori*, but closed-loop control requires immediate access to the *in vivo* drug concentration, which in turn requires real-time processing of sensor data (that is, calibration, data smoothing and baseline correction). To achieve this, we made four key enhancements to our biosensor architecture. First, to eliminate measurement-processing lag (the time offset between when an *in vivo* concentration is reached and when it is reported by the biosensor), we created a real-time analysis program that converts raw electrochemical data from the biosensor into calibrated Dox concentration measurements in real time (see Methods). Second, we used microcapillary tubing to minimize the fluidic transport lag between the animal's bloodstream and the biosensor, resulting in a dead volume of less than 10 μl (see Methods). Third, to ensure measurement accuracy, we implemented a differential measurement algorithm that corrects for any baseline signal drift in real time, providing accurate concentration measurements over the full course of infusion (details in Methods; Supplementary Fig. 2)[24]. Finally, to ensure stable and uninterrupted collection of *in vivo* measurements for several hours, we modified the interior surfaces of the microfluidic flow channel with a heparin-based anticoagulant coating that prevents clot formation, ensuring consistent blood flow through the biosensor throughout the experiment (Supplementary Fig. 3)[36].

With these improvements, our system's biosensor enabled stable and continuous Dox measurement in the bloodstream of live rabbits with a point-to-point sampling interval of 11 s and a measurement lag of only 0.8 min, enabling immediate use of biosensor measurements for closed-loop control (Fig. 1b, bottom). The sensor exhibited a limit of detection of 60 nM Dox in whole blood, with a quantitative

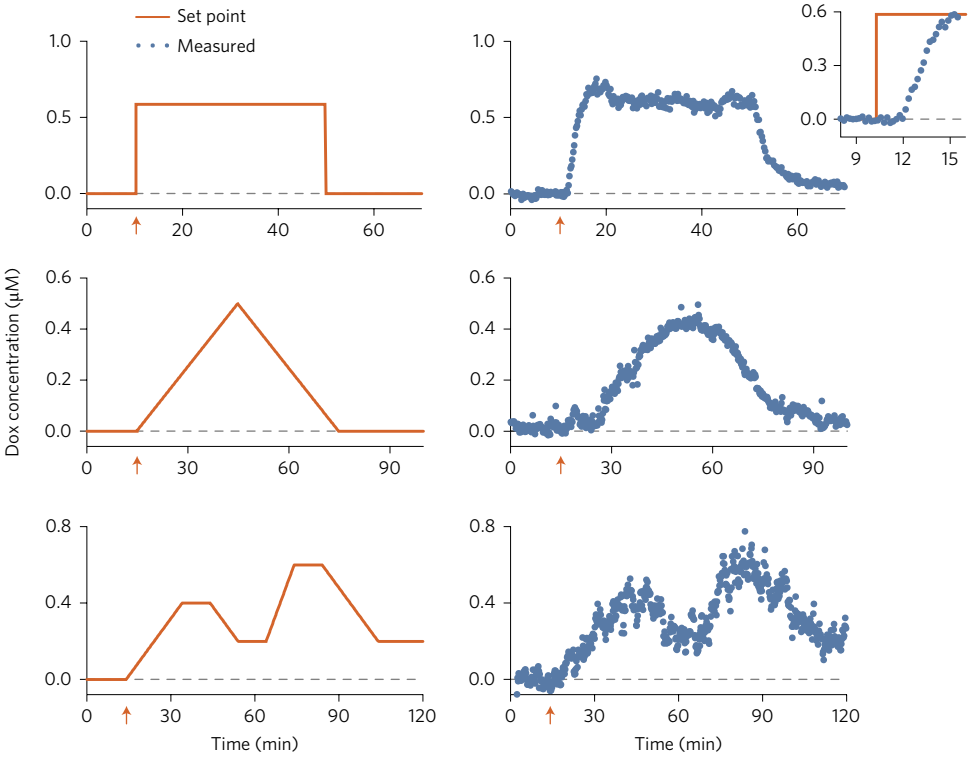

Figure 2 | Closed-loop feedback control of Dox *in vivo*. Our system accurately maintained *in vivo* drug concentrations (blue dots) at the desired set point (orange line) with a response time of 5–10 min in live, conscious New Zealand White rabbits. A variety of concentration profiles can be realized continuously as a function of time. Orange arrows indicate start time of controlled infusion, and each row of panels represents a single experiment in one animal. Inset shows detail of initial rise in upper-right panel. Grey dashed lines highlight 0 μM Dox. Pump output data are shown in Supplementary Fig. 7.

resolution of 50 nM across the sensor's linear response range up to 1 μM (Supplementary Fig. 4; see Methods), making it ideal for use across the clinically relevant plasma concentration range of Dox[31].

We designed our system's control algorithm around a classic PID controller, which calculates the necessary rate of drug infusion by comparing the measured *in vivo* concentration to the desired set point. The PID controller calculates pump output as the weighted sum of three terms: (1) a proportional (*P*) term reflecting the present offset between the measured and target concentrations; (2) an integral (*I*) term which accounts for the accumulated offset between measured and target concentrations over time; and (3) a derivative (*D*) term which predicts future offset based on the rate of measured concentration change. Control behaviour is wholly determined by only three parameters—the proportional, integral and derivative gains (k_p, k_i and k_d)—which determine the relative weight of the *P*, *I* and *D* terms. By tuning the gain settings appropriately, one can obtain a controller that balances response time and stability, even if Dox PK varies unpredictably.

To tune the controller, we evaluated different controller gain settings using a simulated model of the closed-loop system (Fig. 1c). This model mathematically describes the behaviour of each component in the feedback loop, including the biosensor, controller, infusion pump and *in vivo* Dox PK (using a linear time-invariant model of biphasic Dox plasma clearance in rabbits[37]; details in Methods) (Supplementary Fig. 5). Notably, simulations showed that the derivative term decreased the stability of the controller[30], resulting in diminished system performance due to high-frequency noise from our real-time biosensor. We therefore tuned the k_d to zero, in effect forming a proportional–integral (PI) controller. Since PI controllers are intrinsically sensitive to lag, we also modelled all relevant transport-lag and signal-processing delays throughout the loop to account for this (details in Methods). Our model also accounts for nonlinearity arising from saturation of the infusion pump, which can actively increase drug levels by injecting more drug, but must passively rely on the animal's natural clearance rate to lower drug concentration (details in Methods). Using population-averaged Dox PK parameters for rabbits (α- and β-phase plasma clearance rates), we tuned the controller's k_p and k_i gain settings to achieve the shortest response time possible, while avoiding overshoot and steady-state oscillations. We then simulated the controller's performance with these optimized settings and showed that it can achieve stable operation even in the presence of 2.5-fold differences in Dox α-phase clearance rates, the most critical PK parameter determining controller performance (Supplementary Fig. 6). We note that although β-phase clearance rates can also vary significantly, the controller was insensitive to variations in this slower clearance parameter.

Closed-loop control of Dox levels in live rabbits. Using our optimized biosensor and control algorithm, we showed that our system achieves stable, prolonged feedback control of circulating levels of Dox in live, conscious rabbits (Fig. 2). We connected our system to the rabbit's bloodstream through peripheral venous catheters installed in the left and right marginal ear veins, which facilitate simultaneous biosensor measurements and drug infusion (details in Methods). During controlled infusion, our system responded rapidly to step changes in the set point (Fig. 2, top), reaching 95% of the set-point concentration within 7.5 ± 2.9 min of the start of controlled infusion (repeated in four separate rabbits), and remained within 20% (0.1 μM) of the set point throughout the experiment (details in Methods). These set points, representative of typical therapeutic concentrations for humans, were maintained for durations similar to those used during clinical infusions[31]. We also used our system to maintain other dosing profiles as a function of time, including concentration ramp-ups and ramp-downs, and arbitrary combinations of ramps and holds (Fig. 2, middle and bottom, respectively). In all instances, our system dynamically adjusted the Dox infusion

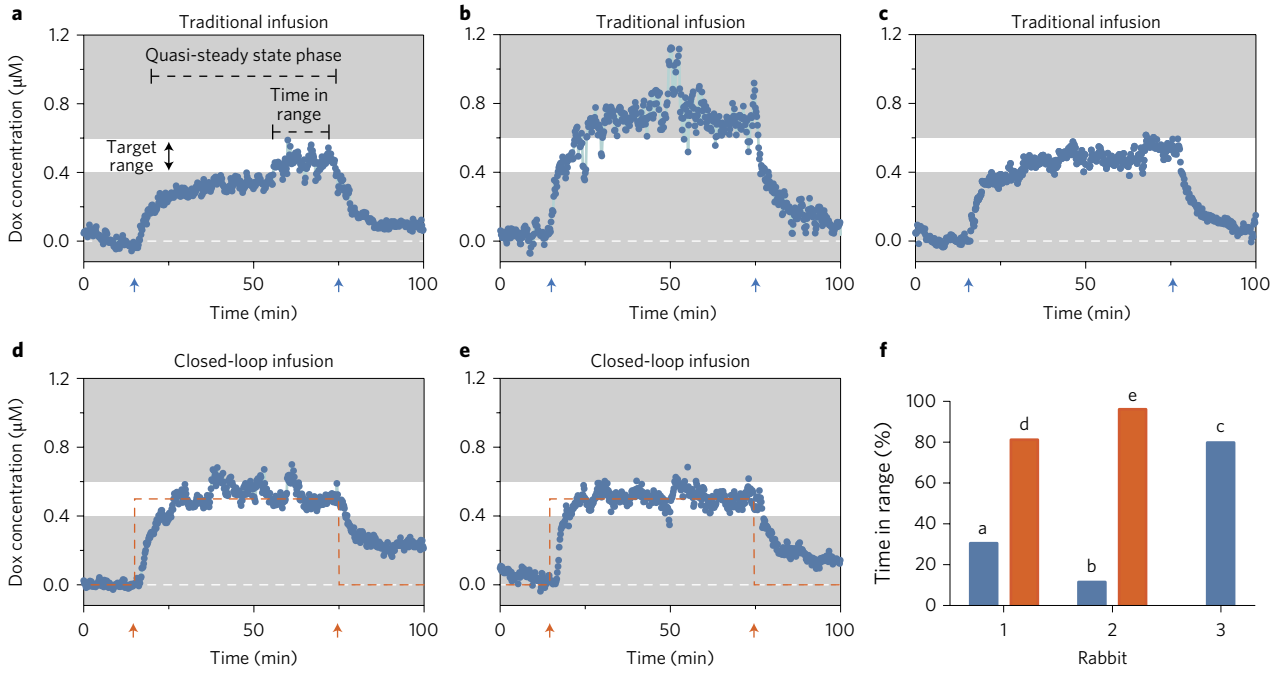

Figure 3 | Closed-loop control of plasma drug levels in animals with varying PK. a–c, Dox plasma concentrations in three different animals over the course of identical BSA-adjusted Dox infusion. The target concentration range is indicated by the white band and the infusion period is demarcated by the blue arrows. **d**,**e**, Dox plasma concentrations during closed-loop infusion. The concentration set point is indicated by the orange dashed line. Data in **d** and **e** are from the same rabbits as **a** and **b**, respectively. Orange arrows indicate start and stop of feedback-controlled infusion. In **a**–**e**, the white dashed lines highlight 0 μM Dox. **f**, Time spent in the target concentration range during infusion. The letters above the bars indicate the panels that show the corresponding infusion data. Pump output data for the measurements shown in **d** and **e** are shown in Supplementary Fig. 7.

rate to meet the designated concentration set point (Supplementary Fig. 7a), remaining within 0.05 μM of the set point throughout the experiment, with a lag time of 5–10 min and minimal oscillation.

Compensating for animal-to-animal PK variability. We next used our closed-loop system to automatically compensate for differences in PK between individual rabbits to maintain a desired set-point concentration. Specifically, we compared our system's dosing performance against the current clinical gold standard for Dox dosing, which is based on normalization to body surface area (BSA)[2,29]. To quantify the extent of PK variability that occurs using BSA-adjusted dosing, we administered three different rabbits with an identical BSA-adjusted dose of Dox. Each animal received a constant 1 h infusion at 11.6 mg m^{-2} h^{-1}, equivalent to typical human therapeutic dosing[29]. Real-time biosensor measurements revealed pronounced variability in plasma levels of Dox across individual rabbits, even when the dosing regimens were normalized by BSA (Fig. 3a–c). Only rabbit 3 (Fig. 3c) achieved the desired plasma level and stayed in the target concentration range for over 80% of the infusion period (white windows in Fig. 3a–e; determination of the target concentration range is described in Methods). The steady-state values of plasma Dox levels in rabbits 1 (Fig. 3a) and 2 (Fig. 3b) were either below or above the desired level, staying within the target concentration range for only 31% and 12% of the infusion period, respectively. It should be noted that the biosensor was independently calibrated immediately before each infusion, ensuring that differences in measured plasma levels were due to PK and not sensor variability (details in Methods).

In contrast, our system automatically and dynamically adjusted infusion rates to achieve the desired Dox concentration in each individual animal (Fig. 3d,e). Under closed-loop infusion control, rabbits 1 and 2 remained within the target concentration range 81% and 96% of the time, respectively (Fig. 3f), a large improvement compared with traditional BSA-adjusted dosing. Importantly, identical k_p and k_i controller gain settings were used for all animals, demonstrating that our system can optimize therapeutic dosing without *a priori* knowledge of an individual's PK.

Correcting for acute drug–drug interactions. Next, we showed that our system can automatically compensate for large perturbations, such as drug–drug interactions, which can cause rapid, unpredictable and dangerous changes in drug PK[38]. Specifically, we co-administered the widely used chemotherapy drug cisplatin (CDDP) to rabbits before Dox infusion[39], which is known to significantly extend the plasma half-life of Dox and increase its peak plasma concentration, due to CDDP-induced changes in liver and kidney function[40]. This interaction was clearly evident when we compared the plasma concentration profile of Dox during Dox-only infusion (Fig. 4a) with that from Dox and CDDP co-administration in the same rabbit one week later (Fig. 4b). Co-administration led to significantly higher plasma levels of Dox over the course of infusion, even though an identical BSA-adjusted Dox dose was given in both cases. Although traditional Dox-only infusion in this rabbit resulted in the target concentration range being achieved for 95% of the time, co-administration with CDDP dramatically reduced the time-in-range to 34%, even when the dose of Dox was normalized identically to BSA (Fig. 4c). In contrast, closed-loop infusion with our system automatically maintained Dox precisely at the desired concentration, even when CDDP was co-administered with Dox (Fig. 4d,e), such that 97% of the infusion time was spent in the target concentration range (Fig. 4f).

Cross-species versatility. We used live Sprague–Dawley rats as a model to show our system's potential for clinical translation, as Dox plasma clearance times in this species[41,42] are nearly identical to humans[31,32]. Using our system in rats rather than rabbits entailed two important modifications. First, rather than using peripheral venous catheters, we connected our system to each rat's bloodstream

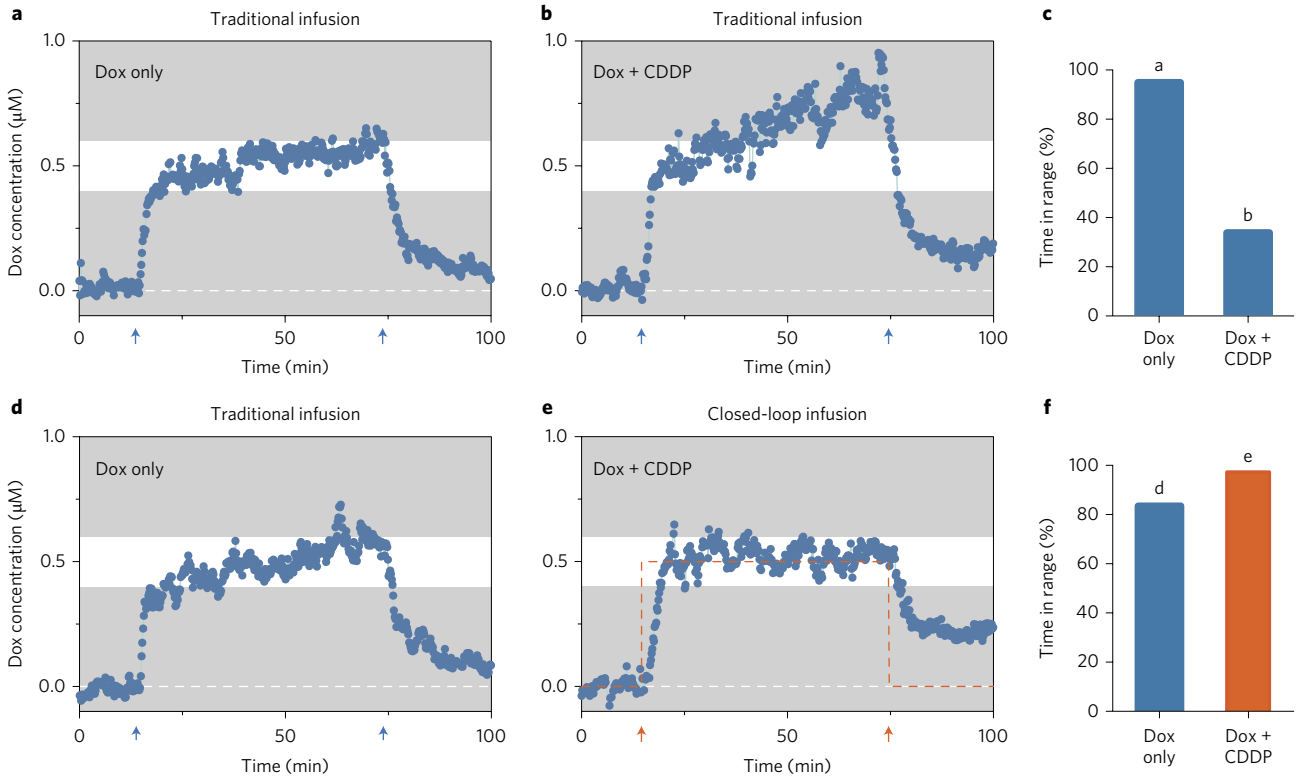

Figure 4 | Closed-loop infusion during acute drug–drug interactions. a,**b**, Dox plasma concentrations in a single rabbit during infusion with Dox alone (**a**) and then Dox infusion when co-administered with CDDP (**b**). **c**, Time in the target range (white bands in **a** and **b**) during infusion. Co-administration with CDDP results in Dox plasma concentrations that fall outside the target range. **d**,**e**, Dox plasma concentrations in a separate rabbit during Dox-only infusion (**d**) and then closed-loop infusion of Dox with co-administered CDDP (**e**). The concentration set point is indicated by the orange dashed line. **f**, Time in the target range (white bands in **d** and **e**) during infusion. Closed-loop Dox infusion maintains the target concentration for the entire duration of infusion, even in the presence of CDDP. Arrows indicate start and end of traditional (blue) or feedback-controlled (orange) Dox infusion; white dashed lines highlight 0 μM Dox. Letters above bars in **c** and **f** indicate the panels that show the corresponding infusion data. Pump output data for the measurements in **e** are shown in Supplementary Fig. 7.

through surgically implanted central venous catheters in the left and right jugular veins; this was necessary because rats lack sufficiently large peripheral blood vessels for catheterization. The use of central venous catheters required that the rats be anaesthetized during infusion (details in Methods). Second, to account for differences in Dox PK relative to rabbits—as well as the rat's tenfold smaller blood volume—we used our mathematical model of our closed-loop system (Fig. 1c) to simulate Dox plasma clearance in rats and thereby identify appropriate k_p and k_i controller settings that enable responsive and stable concentration control (details in Methods). Remarkably, we were able to achieve *in vivo* control performance in rats equivalent to that demonstrated in rabbits by simply adjusting these two parameters, without any further modifications to our system, and reached 95% of the concentration set point within 8.6 min (Fig. 5). We observed slightly elevated Dox plasma levels at the end of the infusion period, due to the considerably longer circulation half-life of Dox in rats. The consistent results achieved from species to species are particularly striking in light of the dramatic physiological differences between the two animal models, including an order-of-magnitude difference in weight, blood volume and Dox clearance times. Moreover, our system functioned identically, whether connected via implanted central venous catheters in fully anaesthetized rats or external peripheral venous catheters in awake rabbits. This versatility suggests that our system could be readily adapted to human use in a variety of clinical contexts, with only minimal modifications—namely, selection of appropriate k_p and k_i gain settings to match Dox PK in humans.

Discussion

In this work, we demonstrated a technology that achieves precise, personalized drug dosing through closed-loop control, based on continuous *in vivo* molecular measurements. As proof of concept, we directly controlled the circulating levels of the chemotherapeutic agent Dox in live animals, demonstrating the capability to reach and maintain a broad range of concentration set points in the bloodstream as a function of time. Our system can automatically adapt in real time to individual physiological differences, compensating for PK variability and even drug–drug interactions. Importantly, because our real-time biosensor uses aptamer probes that can readily be exchanged to measure other drugs (as shown in our previous work[24]), it offers the potential for *in vivo* closed-loop control of any drugs for which aptamer probes are available. Our results with Dox suggest that our system would be well suited for controlling intravenous drugs, for which efficacy and toxicity are closely tied to circulating levels in the blood, including not only chemotherapeutics, but also anticoagulants[43], aminoglycoside antibiotics[44], immunosuppressants[8] and anaesthetics[45]. In addition, the rapid measurement times of our system could eventually make it useful for dosing drugs with rapid PK and pharmacodynamics, especially in situations where patient physiology can change rapidly and unpredictably (for example, during surgery or trauma care).

Although it is beyond the scope of the current study, we believe our system could be readily adapted for human clinical use. As an initial proof of concept, we have successfully controlled Dox concentrations in two mammalian species (rabbits and rats) with dramatically different physiological and PK characteristics. In both species,

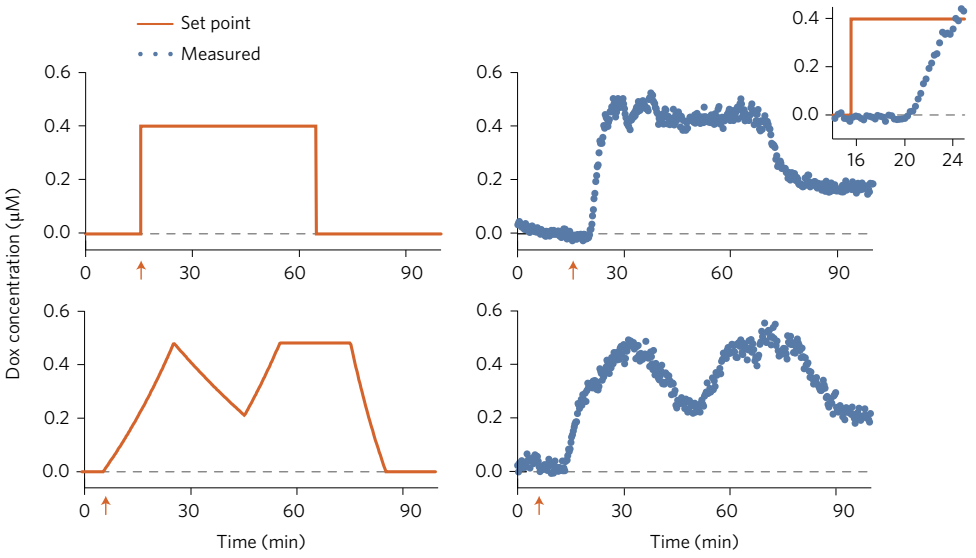

Figure 5 | Closed-loop feedback control of Dox in live, anaesthetized Sprague–Dawley rats. As in rabbits, our system accurately maintained *in vivo* drug concentrations (blue dots) at the desired set point (orange line) with a response time of 5–10 min, and varying concentration profiles can be realized continuously as a function of time; here, two custom concentration profiles are shown. Orange arrows indicate the start time of controlled infusion and each row of panels represents a single experiment in one animal. Inset shows detail of initial rise in upper-right panel. Grey dashed lines highlight 0 μM Dox. Pump output data for these experiments are shown in Supplementary Fig. 7.

we showed that our system can operate over the clinically relevant concentration range of Dox, with stable control over the lengths of time required for clinical infusion protocols (~2 h). Importantly, rats have very similar rates of Dox plasma clearance to humans, suggesting that our system's control algorithm could readily be adapted to control Dox in humans by simply adjusting the controller gain settings. Moreover, these animal models each reflect different potential clinical scenarios: rabbits were treated through external peripheral venous catheters while awake, reflecting typical outpatient infusion protocols, and rats were treated through implanted central venous catheters under general anaesthesia, reflecting conditions for infusion during surgery. Since our system's hardware is entirely *ex vivo* and accesses the bloodstream through standard catheters, we believe our system could safely be employed in humans by taking advantage of existing infusion protocols and equipment.

Ensuring patient safety will also be a critical step in clinical translation. Although the simple PI control algorithm used in this work was sufficient to demonstrate proof-of-concept performance, safe clinical use would require more thorough characterization of nonlinearities in the control system, such as pump output saturation, which could result in PI controller windup[30]. This windup could result in overdosing, but it should be noted that there are well-established anti-windup measures that could be readily implemented in our PI controller[30]. As an additional countermeasure for patient safety, it should be possible to prevent accidental overdosing by configuring hard-wired limits into the infusion pump that trigger shut-off of drug delivery in the event of controller error[46]. We also note that because Dox toxicity manifests on multiple timescales (myelosuppression presents within days[47], while cardiotoxicity manifests after many months[48]), full evaluation of our system's safety for Dox dosing would require follow-up toxicity screening in the months following infusion. This should be accompanied by traditional therapeutic dose monitoring (through periodic blood draws and offline chemical analysis) both during and after Dox administration, to ensure that the biosensor reports accurate Dox concentrations during human use.

Our findings with Dox suggest that our system could offer a powerful tool for the controlled delivery of chemotherapy drugs to paediatric patients. Dox is a first-line chemotherapy drug in childhood liver cancers[49], but its narrow therapeutic window is especially problematic for paediatric patients, who are particularly susceptible to cardiotoxicity from high Dox doses[50]. Unfortunately, Dox PK in children varies widely from patient to patient due to differences in age and degree of physical development. The current clinical standard of BSA normalization has delivered no improvement in therapeutic efficacy or safety for Dox treatment in children[51]. Based on our success with rats and rabbits, we believe our system could overcome this PK variability and thus enable optimal, individualized chemotherapeutic dosing.

We note a number of practical performance limitations arising from our system's existing configuration. First, PI control is sensitive to time lags throughout the feedback loop. The use of an *ex vivo* biosensor chip results in small but unavoidable time delays arising from fluidic transport lag as blood flows from the animal's bloodstream to the chip. Careful optimization of the fluidics enabled us to achieve sub-minute transport lag, but this places an upper bound on how quickly the controller can detect and respond to changes in *in vivo* concentration. We note that the target binding kinetics of our existing Dox aptamer (described in detail in our previous work[24]) are sufficiently fast to detect and control concentration changes for Dox, but this would be an important consideration for evaluating aptamers for new drug targets. Faster control performance could also be obtained by improving the algorithm itself—for example, by including derivative action in the controller for true PID control. However, this would require careful noise-rejection schemes to ensure stable control performance. Furthermore, since our system can only actively increase drug concentration, it may not be well suited for controlling both rising and falling concentration profiles of drugs with very slow PK. We also note that our PI control algorithm, which is tuned using a linear model of Dox PK, would not account for nonlinearities that could arise in real-world use across a wider range of patients and drugs (such as concentration-dependent drug elimination rates). More sophisticated control algorithms, such as model predictive control, could account for such nonlinearity and automatically self-adapt to PK changes from patient to patient, and would therefore not require manual re-tuning of the controller; these have been thoroughly investigated in the context of controlled insulin infusion[52].

We envision a number of potential improvements that could further expand the clinical utility of our system. First, the current system is designed to control infusion based on only measurements of free drug molecules in the blood, but levels of metabolites and plasma-protein-bound drug molecules can also be important indicators of pharmacological activity for certain drugs, including Dox[53]. Thus, it would be useful to integrate multiple aptamer probes that make it possible to control infusion based on combined measurements of free drug as well as metabolites or drug–protein complexes. This would require development of metabolite-specific aptamers, which could be readily multiplexed onto our biosensor using established methods[54], as well as multi-input control algorithms[55]. Second, we designed our system to regulate infusion based on measured levels of drug in the intravascular compartment, which is appropriate for drugs whose efficacy and toxicity are closely correlated with plasma concentration. To control drugs with more complex tissue distribution and metabolism pathways, future versions of our system could utilize PK models that predict drug concentration in the target organ, a strategy that is being employed in artificial pancreas systems[56]. Finally, in its present configuration, our system is an *ex vivo* system that would be well suited for use in clinical settings. However, future iterations of the system could incorporate implantable sensors[57] and infusion devices[58] to enable continuous, minimally invasive dose regulation as a patient goes about their daily activities. With such advances, we believe this technology could potentially transform the treatment of chronic conditions.

Methods

Study design. The objectives of our study were twofold. First, we sought to demonstrate the proof-of-concept capability to directly control circulating concentrations of therapeutic agents in live New Zealand White rabbits and Sprague–Dawley rats, using Dox as a model. Second, we aimed to use this closed-loop control to adjust Dox administration in rabbits to automatically compensate for PK variability, both between animals and within the same animal due to drug–drug interactions. To evaluate controller performance, Dox concentrations were measured directly in the animals' bloodstreams using our real-time biosensor. To evaluate PK variability, we measured the circulating concentration of Dox in multiple rabbits undergoing identical BSA-adjusted infusions of Dox, as well as in rabbits undergoing identical infusions of Dox before and after CDDP administration. For PK variability experiments, rabbits were used instead of rats because drug monitoring and control can be performed as a non-terminal survival procedure in rabbits, enabling comparison across multiple experiments in the same animal. Individual animals were selected randomly for each experiment. Blinding was not applicable to this study. For all *in vivo* data, each graph corresponds to a single animal, and each data point corresponds to a single differential biosensor measurement.

Sensor fabrication. Sensor fabrication was performed according to our previous protocol, described in detail in ref. [24] (Supplementary Fig. 1). To prevent clot formation in the sensor chips during exposure to whole blood, a commercial heparin surface-coating kit[36] (Harvard Apparatus) was used to treat the inner surfaces of the assembled sensor channel.

Aptamer probe preparation and immobilization. The Dox-specific aptamer probe was synthesized by LGC Biosearch Technologies with the following sequence: 5′-(HS-$(CH_2)_6$)$_3$-ACCATCTGTGTAAGGGGTA AGGGGTGGT-MB-3′. The design rationale for this probe is described in detail in ref. [24]. The probe was tri-thiolated[59] at the 5′ end to facilitate stable immobilization and self-assembly on the gold working electrodes and conjugated with a methylene blue (MB) redox label at the 3′ end to enable target-binding-induced charge transfer modulation. Probe preparation and immobilization were otherwise identical to ref. [24].

Fluidic instrumentation. All flow to and from our system was controlled via syringe pumps (PhD 2000, Harvard Apparatus). The sensor chip input port was connected to a 24-gauge intravenous catheter (Insyte Autoguard, Beckton Dickinson) for rabbit studies via a 15 cm length of 0.20 mm inner diameter fluorinated ethylene propylene tubing (IDEX), resulting in a total fluidic dead volume of 9 µl between the rabbit bloodstream and the sensor chip. In rats, the same length of fluorinated ethylene propylene tubing was interfaced with the rat's jugular vein via 1 cm of 0.05 cm inner diameter silicone elastomer tubing (Silastic, Dow Corning) and 5 cm of 0.03 cm silicone elastomer tubing, resulting in a total dead volume of 10.5 µl. A 10 ml syringe loaded with 1 × saline-sodium citrate (SSC) supplemented with 100 IU ml^{-1} heparin (Savmart Pharmaceuticals) was placed in a pump and connected to the buffer port on the sensor chip via a 30 cm length of Tygon tubing (Saint-Gobain Performance Plastics; 1.78 mm outer diameter and 1.02 mm inner diameter). The sensor chip output port was connected to a primed 20 ml 'waste' syringe placed in a second pump via 1.65 mm outer diameter and 0.762 mm inner diameter silicone tubing (NewAge Industries). To monitor flow rates in real time, we used a Mitos Flow Rate Sensor (Dolomite Microfluidics) in-line between the output port and waste syringe pump. The buffer layer was established by engaging the buffer pump at 0.331 ml h^{-1}, while sample was simultaneously and continuously drawn into the device by engaging the waste pump at 1.654 ml h^{-1}.

Voltammetry. Electrochemical measurements were conducted with a PalmSens EmStat2 USB-connected potentiostat (Palm Instruments BV). Biosensor chips were connected to the potentiostat via an 8-pin card edge connector. The chip contained six working electrodes positioned along the flow channel[24]; all measurements performed in this work used the working electrode positioned 17 mm downstream from the flow junction. Square-wave voltammetry scans were performed at interrogation frequencies of 10 Hz and 100 Hz, with a square-wave pulse amplitude of 30 mV and potential steps of 10 mV and 1 mV, respectively, resulting in an average scan period of 5.5 s. A potential range of 160 mV to −240 mV (with respect to a platinum reference electrode) was used to capture the full redox current peak of methylene blue. In cases where reference potential drift occurred, the scan range was adjusted until the methylene blue redox peak occurred in the centre of the range.

Signal processing. A custom peak-fitting script was used to fit the square-wave voltammetry scans with a Gaussian curve on a linear baseline. For each frequency, the fitted peak currents were normalized to an initial baseline peak current to calculate signal gain. To correct for signal drift over time, the differential measurement scheme described in detail in ref. [24] was implemented in real time using the signal gains at 100 Hz and 10 Hz square-wave voltammetry frequencies at each time point. The differential signal at each time point was calculated as the difference of the 100 Hz and 10 Hz signal gains at that time point, divided by their average (Supplementary Fig. 2). To correct for signal artefacts caused by blood flow fluctuations, induced by animal motion during the rabbit experiment (Fig. 2, bottom panel), a linear correction factor based on the measured flow rate was applied to the differential signal.

Sensor calibration and characterization. To convert electrochemical current measurements to concentration values, we obtained a dose–response curve by exposing the biosensor chip to Dox (LC Laboratories) concentrations ranging from 250 nM to 8 µM in rabbit whole blood flowing at the rate described above (Supplementary Fig. 4). At each concentration, the biosensor signal was permitted to equilibrate and the subsequent 30 points were averaged as the reported values. A dose–response curve was obtained by fitting the differential signal gain at each Dox titration to a Langmuir isotherm, resulting in an apparent dissociation constant (K_d) of 1.68 ± 0.03 µM (mean ± s.e.m.), which was used to calibrate all sensor chips. Unless otherwise noted, all biosensor chips were individually calibrated in rabbit whole blood immediately before *in vivo* measurements to determine their chip-specific saturation binding values (B_{max}), with the exception of the biosensor chips used to collect the data for the figures in the top row of Fig. 2 and Fig. 5, which were calibrated with an estimated B_{max} of 0.9, based on the dose–response curve described above.

Based on the dose-response measurements described above, sensor limit of detection (LOD) was defined as the concentration producing a signal three-baseline standard deviations (σ_b) above zero:

$$\mathrm{LOD} = K_d \frac{3\sigma_b}{B_{max} - 3\sigma_b}$$

The sensor's quantitative resolution (QR) was defined as the ratio of the measurement uncertainty (σ_m) to the assay's analytical sensitivity (A, the slope of the sensor's response function in the linear range from 0.1–1 µM):

$$\mathrm{QR} = \sigma_m / A$$

Real-time analysis and control program. To facilitate real-time measurement, dose calculation and pump control, a custom analysis and control program was written in MATLAB R2013b (Mathworks). The program performs three key functions: (1) retrieving and converting raw electrochemical data from the potentiostat into calibrated concentration measurements; (2) calculating the necessary infusion rate based on these measurements and the user-input concentration set point, using a discrete implementation of the parallel PI control algorithm; and (3) communicating with the infusion pump to adjust the drug infusion rate. In addition, the program provides a real-time graphical plotting interface, enabling the user to observe concentration measurements and controller output.

Control algorithm design and implementation. The control algorithm used by our system takes the traditional form of a parallel PI controller:

$$U(t) = k_p e(t) + k_i \int_0^t e(\tau) d\tau$$

where $U(t)$ is the controller output dose (nmol) at time t, k_p is the proportional gain parameter (mM), $e(t)$ is the error (the difference between measured concentration and set-point concentration at time t; μM), and k_i is the integral gain parameter ($mM\,s^{-1}$). The control algorithm was implemented in a discrete form, with a fixed sampling time of 5 s.

Control system modelling, simulation and tuning. The dynamical systems simulation software Simulink (Mathworks) was used to model the feedback loop comprising the animal PK, real-time biosensor and PI controller, as well as all relevant transport and signal processing delays in the system. The PK of Dox in rabbits and rats was modelled as a biphasic concentration decay, with decay constants α and β and respective weighting constants W_α and W_β:

$$\frac{C(t)}{C_0} = W_\alpha \exp(-\alpha t) + W_\beta \exp(-\beta t)$$

where $C(t)$ is the drug concentration in the bloodstream at time t and C_0 is the initial concentration. An empirically determined constant dilution volume V_D was incorporated to account for dilution of the drug in the bloodstream. This semi-empirical PK model accurately recreated measured Dox PK in rabbits (Supplementary Fig. 5). To model the real-time biosensor, we incorporated empirical terms to account for the fluidic transport delay from the animal's bloodstream to the sensor, the sensor's fixed sampling rate and the sensor's temporal response to changes in Dox concentration due to aptamer-target binding and unbinding (fitted from sensor step-response data).

With the full feedback loop described in the model, we used Simulink's built-in PID tuning functionality to determine k_p and k_i controller gain settings that produced the most rapid response time and minimized both overshoot and oscillation about the set point for a range of α-phase clearance rates (half-lives ranging from 1.5 to 4.0 min; Supplementary Fig. 6). The relatively slow β-phase clearance rates (with a half-life ranging from 0.5 to 1.5 h in rabbits) had minimal impact on initial controller step response. Importantly, we modelled saturation of the pump output to allow non-negative infusion rates only, reflecting the fact that we cannot actively lower the concentration of drug in the bloodstream (that is, we cannot infuse a 'negative' dose of drug); this accounts for the real-world asymmetry of our control system, which can only rely on the animal's natural drug clearance rate to lower drug concentration. To adjust the simulation for control in rats (Fig. 5), we simply modified the Dox PK parameters in the model to reflect the slower clearance rates and smaller blood volume in rats, and re-tuned the controller to obtain new controller gain settings for use in rats.

Live animal studies. Live animal studies using New Zealand White rabbits were performed according to our protocol titled '*In vivo* small molecule detection (rabbits)', approved by the University of California, Santa Barbara (UCSB) Institutional Animal Care and Use Committee (IACUC) and assigned protocol number 859. All rabbits used in this work were male and purchased from Charles River Laboratories. Rabbits were acclimated to the facility for at least one week after arrival and observed for abnormal health conditions before experiments were performed. Rabbits were treated with aspirin (CVS) ($10\,mg\,kg^{-1}$ by mouth, cumulative) and clopidogrel (Henry Schein) ($10\,mg\,kg^{-1}$ by mouth, cumulative) over the four days leading up to and including the day of the experiment to prevent formation of clots in the catheter, tubing and chip during blood draws[60]. Immediately before the experiment, rabbits were partially sedated with acepromazine (Henry Schein) ($1\,mg\,kg^{-1}$ intramuscular injection). Rabbits were placed in rabbit restrainers to prevent them from damaging or disturbing their catheters. To facilitate catheter access to the marginal ear veins, the rabbits' ears were shaved and a topical anaesthetic (EMLA lidocaine/prilocaine cream, MedVet) was applied 15 min before catheterization. Cannulation was performed in the marginal vein of both ears (Insyte Autoguard Shielded IV Catheter, Becton–Dickinson). To prevent clot formation in the catheters, tubing and sensor chip, an initial dose of $300\,IU\,kg^{-1}$ heparin was injected via each catheter, followed by hourly doses of $150\,IU\,kg^{-1}$ administered via the right ear vein catheter. Following catheterization and heparin administration, 2.5 ml of blood was drawn for sensor calibration. After calibration, capillary tubing (0.02 cm inner diameter fluorinated ethylene propylene tubing, IDEX) was inserted into the left ear vein catheter and blood was drawn continuously from the catheter through the sensor chip at a rate of $1.323\,ml\,h^{-1}$. Bolus injections, continuous infusions and controlled infusions of Dox and CDDP (Western Medical Supply) were all administered via the right ear vein catheter. Continuous and controlled infusions were injected by a syringe pump from a 5 ml syringe connected to the catheter via a 30 cm length of polytetrafluoroethylene (PTFE) tubing (Cole–Parmer; 0.76 mm outer diameter and 0.30 mm inner diameter). The catheters for infusion and measurement were placed such that the injected drug passed through the heart and into circulation before being withdrawn for measurement. At the conclusion of experiments, rabbits were euthanized via intravenous Euthasol (Virbac Animal Health) injection if they received CDDP during the experiment and/or their cumulative dose of Dox across all experiments exceeded $1\,mg\,kg^{-1}$; otherwise, they were returned to their cages for recovery and use in subsequent experiments. In total, we used 14 rabbits during the development and testing of our system and we present data from 8 rabbits in the manuscript.

Live animal studies using Sprague–Dawley rats were performed under our '*In vivo* small molecule detection' protocol, similarly approved by the UCSB IACUC and assigned protocol number 824. All rats used in this work were male and purchased from Charles River Laboratories. The rat surgical setup protocol, including anaesthetization, catheter placement, heparin administration, Dox bolus administration and euthanasia, is identical to the protocol described in ref. [24], with the addition that controlled infusion of Dox was administered into the right jugular vein catheter using the same setup described for rabbits. We used a total of six rats during the development and testing of our system, and we present data from two rats in the manuscript.

Controlled infusions of Dox for rats and rabbits were given at a concentration of 2 mM. For continuous open-loop infusion experiments in rabbits, Dox concentration and infusion rates were selected such that all rabbits would receive the same BSA-adjusted dose at an infusion rate of $11.6\,mg\,m^{-2}\,h^{-1}$ for exactly 1 h. BSA (in m^2) was calculated for dose normalization according to the equation:

$$\mathrm{BSA} = \frac{K \times m^{2/3}}{10,000}$$

where m is the animal's mass in grams, and $K = 9.9$ for rabbits[61] or 9.46 for rats[62]. CDDP, when administered, was given to achieve a total dose of $4\,mg\,kg^{-1}$ as a single bolus injection, at a concentration of $1\,mg\,ml^{-1}$, 2–4 h before Dox infusion.

Step-response rise time calculation and infusion analysis. To quantify controller performance *in vivo*, we calculated the time required for the controller to reach 95% of its set-point step response, with the starting time defined as when feedback control was activated. For these calculations, sensor data were smoothed to minimize the impact of high-frequency noise. Step-response profiles from four separate rabbit experiments were analysed to calculate mean and standard deviation. For more complicated set-point waveforms, including ramps and holds, controller performance was quantified by calculating the absolute deviation of the measured concentration from the set-point concentration at each time point. To correct for controller lag, the measured response was time-shifted by the controller lag time before calculating the deviation from the set point.

In each rabbit, the plasma concentration profile was characterized by a rapid rise (drug distribution phase, 1–5 min after start of infusion), a subsequent slow linear increase in concentration over the remainder of the infusion time (quasi-steady state, qSS, 6–60 min after start of infusion), and a rapid decrease to a slightly elevated baseline concentration after cessation of infusion. We defined the target concentration range as a window whose centre was the average concentration during the qSS phase across all three rabbits in Fig. 3a–c (each receiving an identical hour-long $11.6\,mg\,m^2\,h^{-1}$ Dox-only infusion) and whose width was the average standard deviation of the qSS-phase concentration in a single animal. We calculated this target range to be 0.5 ± 0.1 μM. Percent time in target range was defined as the percentage of the qSS phase during which the measured *in vivo* concentration was within the target concentration range.

Code availability. All custom MATLAB code used to generate the findings of this study is freely available at http://github.com/petermage/iv-feedback-gui. Code is available for use under the BSD-3-Clause Licence.

Data availability. The authors declare that all data supporting the findings of this study are available within the paper and its Supplementary Information.

Received 12 October 2016; accepted 29 March 2017; published 10 May 2017

References

1. Baker, S. D. *et al.* Role of body surface area in dosing of investigational anticancer agents in adults, 1991–2001. *J. Natl Cancer I.* **94,** 1883–1888 (2002).
2. Gurney, H. How to calculate the dose of chemotherapy. *Brit. J. Cancer* **86,** 1297–1302 (2002).
3. Khalil, F. & Läer, S. Physiologically based pharmacokinetic modeling: methodology, applications, and limitations with a focus on its role in pediatric drug development. *J. Biomed. Biotechnol.* **2011,** 907461 (2011).
4. Mathijssen, R. H. J. *et al.* Flat-fixed dosing versus body surface area based dosing of anticancer drugs in adults: does it make a difference? *Oncologist* **12,** 913–923 (2007).
5. Muller, P. Y. & Milton, M. N. The determination and interpretation of the therapeutic index in drug development. *Nat. Rev. Drug Discov.* **11,** 751–761 (2012).
6. Gao, B., Klumpen, H.-J. & Gurney, H. Dose calculation of anticancer drugs. *Expert Opin. Drug Met.* **4,** 1307–1319 (2008).

7. Undevia, S. D., Gomez-Abuin, G. & Ratain, M. J. Pharmacokinetic variability of anticancer agents. *Nat. Rev. Cancer* **5,** 447–458 (2005).
8. Johnston, A. & Holt, D. W. Therapeutic drug monitoring of immunosuppressant drugs. *Brit. J. Clin. Pharmaco.* **47,** 339–350 (1999).
9. van Gelder, T., van Schaik, R. H. & Hesselink, D. A. Pharmacogenetics and immunosuppressive drugs in solid organ transplantation. *Nat. Rev. Nephrol.* **10,** 725–731 (2014).
10. Burns, M. Management of narrow therapeutic index drugs. *J. Thromb. Thrombolys.* **7,** 137–143 (1999).
11. Cohen, M. R. Pharmacists' role in ensuring safe and effective hospital use of insulin. *Am. J. Health-Syst. Ph.* **67,** S17–S21 (2010).
12. Kanto, J. & Gepts, E. Pharmacokinetic implications for the clinical use of propofol. *Clin. Pharmacokinet.* **17,** 308–326 (1989).
13. Relling, M. V. & Evans, W. E. Pharmacogenomics in the clinic. *Nature* **526,** 343–350 (2015).
14. Momper, J. D. & Wagner, J. A. Therapeutic drug monitoring as a component of personalized medicine: applications in pediatric drug development. *Clin. Pharmacol. Ther.* **95,** 138–140 (2014).
15. Zanger, U. M. Pharmacogenetics—challenges and opportunities ahead. *Front. Pharmacol.* **1,** 112 (2010).
16. Wang, B., Canestaro, W. J. & Choudhry, N. K. Clinical evidence supporting pharmacogenomic biomarker testing provided in US Food and Drug Administration drug labels. *JAMA Intern. Med.* **174,** 1938–1944 (2014).
17. Touw, D. J., Neef, C., Thomson, A. H. & Vinks, A. A. Cost-effectiveness of therapeutic drug monitoring: a systematic review. *Ther. Drug Monit.* **27,** 10–17 (2005).
18. Swen, J. J. *et al.* Translating pharmacogenomics: challenges on the road to the clinic. *PLoS Med.* **4,** 1317–1324 (2007).
19. DiFrancesco, R. *et al.* Quality assessment for therapeutic drug monitoring in AIDS Clinical Trials Group (ACTG 5146): a multicenter clinical trial. *Ther. Drug Monit.* **32,** 458–466 (2010).
20. Klonoff, D. C. Smart sensors for maintaining physiologic homeostasis. *J. Diabetes Sci. Technol.* **5,** 470–475 (2011).
21. Uemura, K. & Sugimachi, M. Automated cardiovascular drug infusion system to control hemodynamics. *Adv. Biomed. Eng.* **2,** 32–37 (2013).
22. Struys, M. M. *et al.* Comparison of closed-loop controlled administration of propofol using Bispectral Index as the controlled variable versus 'standard practice' controlled administration. *Anesthesiology* **95,** 6–17 (2001).
23. Doyle, F. J., Huyett, L. M., Lee, J. B., Zisser, H. C. & Dassau, E. Closed-loop artificial pancreas systems: engineering the algorithms. *Diabetes Care* **37,** 1191–1197 (2014).
24. Ferguson, B. S. *et al.* Real-time, aptamer-based tracking of circulating therapeutic agents in living animals. *Sci. Transl. Med.* **5,** 213ra165 (2013).
25. Chatelut, E. *et al.* Dose banding as an alternative to body surface area-based dosing of chemotherapeutic agents. *Brit. J. Cancer* **107,** 1100–1106 (2012).
26. Eksborg, S., Strandler, H.-S., Edsmyr, F., Näslund, I. & Tahvanainen, P. Pharmacokinetic study of IV infusions of adriamycin. *Eur. J. Clin. Pharmacol.* **28,** 205–212 (1985).
27. Dobbs, N. A. *et al.* Gender affects doxorubicin pharmacokinetics in patients with normal liver biochemistry. *Cancer Chemoth. Pharm.* **36,** 473–476 (1995).
28. Elis, A. *et al.* Doxorubicin in lymphoma: association between pharmacokinetic variability and clinical response. *Ther. Drug Monit.* **32,** 50–52 (2010).
29. Barpe, D. R., Rosa, D. D. & Froehlich, P. E. Pharmacokinetic evaluation of doxorubicin plasma levels in normal and overweight patients with breast cancer and simulation of dose adjustment by different indexes of body mass. *Eur. J. Pharm. Sci.* **41,** 458–463 (2010).
30. Ang, K. H., Chong, G. & Li, Y. PID control system analysis, design, and technology. *IEEE T. Contr. Syst. T.* **13,** 559–576 (2005).
31. Greene, R. F., Collins, J. M., Jenkins, J. F., Speyer, J. L. & Myers, C. E. Plasma pharmacokinetics of adriamycin and adriamycinol: implications for the design of *in vitro* experiments and treatment protocols. *Cancer Res.* **43,** 3417–3421 (1983).
32. Camaggi, C. M. *et al.* Epirubicin and doxorubicin comparative metabolism and pharmacokinetics. A cross-over study. *Cancer Chemoth. Pharm.* **21,** 221–228 (1988).
33. Mross, K. *et al.* Pharmacokinetics and metabolism of epidoxorubicin and doxorubicin in humans. *J. Clin. Oncol.* **6,** 517–526 (1988).
34. Mross, K., Mayer, U., Hamm, K., Burk, K. & Hossfeld, D. K. Pharmacokinetics and metabolism of iodo-doxorubicin and doxorubicin in humans. *Eur. J. Clin. Pharmacol.* **39,** 507–513 (1990).
35. Schoukroun-Barnes, L. R. *et al.* Reagentless, structure-switching, electrochemical aptamer-based sensors. *Annu. Rev. Anal. Chem.* **9,** 163–181 (2016).
36. Thorslund, S., Sanchez, J., Larsson, R., Nikolajeff, F. & Bergquist, J. Functionality and stability of heparin immobilized onto poly(dimethylsiloxane). *Colloid. Surface B* **45,** 76–81 (2005).
37. Maniez-Devos, D. M., Baurain, R., Trouet, A. & Lesne, M. Doxorubicin pharmacokinetics in the rabbit. *J. Pharmacol.* **16,** 159–169 (1985).
38. Scripture, C. D. & Figg, W. D. Drug interactions in cancer therapy. *Nat. Rev. Cancer* **6,** 546–558 (2006).
39. Watanabe, K. Current chemotherapeutic approaches for hepatoblastoma. *Int. J. Clin. Oncol.* **18,** 955–961 (2013).
40. Najjar, T. A. O. & Saad, S. Y. Effect of treatment schedule on the toxicity and pharmacokinetics of cisplatin-doxorubicin combination in rabbits. *J. Egypt. Nat. Cancer I.* **12,** 259–265 (2000).
41. Rahman, A., Carmichael, D., Harris, M. & Roh, J. K. Comparative pharmacokinetics of free doxorubicin and doxorubicin entrapped in cardiolipin liposomes. *Cancer Res.* **46,** 2295–2299 (1986).
42. Ueda, Y. *et al.* Comparison of efficacy, toxicity and pharmacokinetics of free adriamycin and adriamycin linked to oxidized dextran in rats. *Chem. Pharm. Bull.* **37,** 1639–1641 (1989).
43. Bendetowicz, A. V, Béguin, S., Caplain, H. & Hemker, H. C. Pharmacokinetics and pharmacodynamics of a low molecular weight heparin (enoxaparin) after subcutaneous injection, comparison with unfractionated heparin—a three way cross over study in human volunteers. *Thromb. Haemostasis* **71,** 305–313 (1994).
44. Barbour, A., Scaglione, F. & Derendorf, H. Class-dependent relevance of tissue distribution in the interpretation of anti-infective pharmacokinetic/pharmacodynamic indices. *Int. J. Antimicrob. Ag.* **35,** 431–438 (2010).
45. Absalom, A. R., Mani, V., De Smet, T. & Struys, M. M. R. F. Pharmacokinetic models for propofol—defining and illuminating the devil in the detail. *Brit. J. Anaesth.* **103,** 26–37 (2009).
46. Williams, C. K. & Maddox, R. R. Implementation of an i.v. medication safety system. *Am. J. Health-Syst. Ph.* **62,** 530–536 (2005).
47. Hortobágyi, G. N. Anthracyclines in the treatment of cancer. *Drugs* **54,** (Suppl. 4) 1–7 (1997).
48. Singal, P. K. & Iliskovic, N. Doxorubicin-induced cardiomyopathy. *N. Engl. J. Med.* **339,** 900–905 (1998).
49. Minotti, G., Menna, P., Salvatorelli, E., Cairo, G. & Gianni, L. Anthracyclines: molecular advances and pharmacologic developments in antitumor activity and cardiotoxicity. *Pharmacol. Rev.* **56,** 185–229 (2004).
50. Fulbright, J. M., Huh, W., Anderson, P. & Chandra, J. Can anthracycline therapy for pediatric malignancies be less cardiotoxic? *Curr. Oncol. Rep.* **12,** 411–419 (2010).
51. Hutson, J. R. *et al.* Pharmacokinetic and pharmacogenetic determinants and considerations in chemotherapy selection and dosing in infants. *Expert Opin. Drug Met.* **8,** 709–722 (2012).
52. Grosman, B., Dassau, E., Zisser, H. C., Jovanovic, L. & Doyle, F. J. Zone model predictive control: a strategy to minimize hyper- and hypoglycemic events. *J. Diabetes Sci. Technol.* **4,** 961–975 (2010).
53. Greenblatt, D. J., Sellers, E. M. & Koch-Weser, J. Importance of protein binding for the interpretation of serum or plasma drug concentrations. *J. Clin. Pharmacol.* **22,** 259–263 (1982).
54. Pavlovic, E. *et al.* Microfluidic device architecture for electrochemical patterning and detection of multiple DNA sequences. *Langmuir* **24,** 1102–1107 (2008).
55. Turksoy, K., Bayrak, E. S., Quinn, L., Littlejohn, E. & Cinar, A. Multivariable adaptive closed-loop control of an artificial pancreas without meal and activity announcement. *Diabetes Technol. The.* **15,** 386–400 (2013).
56. Magni, L. *et al.* Run-to-run tuning of model predictive control for type 1 diabetes subjects: *in silico* trial. *J. Diabetes Sci. Technol.* **3,** 1091–1098 (2009).
57. Ho, J. S. *et al.* Wireless power transfer to deep-tissue microimplants. *Proc. Natl Acad. Sci. USA* **111,** 7974–7979 (2014).
58. Farra, R. *et al.* First-in-human testing of a wirelessly controlled drug delivery microchip. *Sci. Transl. Med.* **4,** 122ra21 (2012).
59. Phares, N., White, R. J. & Plaxco, K. W. Improving the stability and sensing of electrochemical biosensors by employing trithiol-anchoring groups in a six-carbon self-assembled monolayer. *Anal. Chem.* **81,** 1095–1100 (2009).
60. Herbert, J. M. *et al.* The antiaggregating and antithrombotic activity of clopidogrel is potentiated by aspirin in several experimental models in the rabbit. *Thromb. Haemostasis* **80,** 512–518 (1998).
61. Zehnder, A. M., Hawkins, M. G., Trestrail, E. A., Holt, R. W. & Kent, M. S. Calculation of body surface area via computed tomography-guided modeling in domestic rabbits (*Oryctolagus cuniculus*). *Am. J. Vet. Res.* **73,** 1859–1863 (2012).
62. Gilpin, D. A. Calculation of a new Meeh constant and experimental determination of burn size. *Burns* **22,** 607–611 (1996).

Acknowledgements

We are grateful for the financial support of the Garland Initiative, Army Research Office (W911NF-10-2-0114, W911QY-15-C-0026) and the W. M. Keck Foundation Medical Research Program. We thank B. Eisenhower, D. Hoggarth, J. Somerson, D. Mamerow, A. Pressman, G. Marcus, S. Hall, M. Eisenstein, M. Nakamoto, K. Plaxco and F. Doyle for helpful discussions. We also thank A. Griffin, R. Wynn, and M. Garcia at the UCSB Animal Resource Center for their technical expertise and assistance with the animal studies.

Author contributions

B.S.F. and H.T.S. conceived of the project. P.L.M. and B.S.F. designed the experiments, fabricated the sensors and created the control and simulation software. P.L.M. directed the animal studies, performed the controller simulations and analysed the data. D.M. and K.L.P. performed all animal procedures in the studies. T.E.K. assisted in design of, provided supervision for, and wrote the protocols for the animal studies. P.L.M. and H.T.S wrote and edited the manuscript. All authors discussed the results and commented on the manuscript.

Additional information

Supplementary information is available for this paper.

Reprints and permissions information is available at www.nature.com/reprints.

Correspondence and requests for materials should be addressed to H.T.S.

How to cite this article: Mage, P. L. *et al.* Closed-loop control of circulating drug levels in live animals. *Nat. Biomed. Eng.* **1,** 0070 (2017).

Competing interests

The authors declare no competing financial interests.